

Efficient and Accurate Modeling of Multiwavelength Propagation in SOAs: A Generalized Coupled-Mode Approach

Cristian Antonelli, Antonio Mecozzi, *Fellow, IEEE, Fellow, OSA*, Wangzhe Li, and Larry A. Coldren, *Life Fellow, IEEE, Fellow, OSA*

Abstract—We present a model for multiwavelength mixing in semiconductor optical amplifiers (SOAs) based on coupled-mode equations. The proposed model applies to all kinds of SOA structures, takes into account the longitudinal dependence of carrier density caused by saturation, it accommodates an arbitrary functional dependencies of the material gain and carrier recombination rate on the local value of carrier density, and is computationally more efficient by orders of magnitude as compared with the standard full model based on space-time equations. We apply the coupled-mode equations model to a recently demonstrated phase-sensitive amplifier based on an integrated SOA and prove its results to be consistent with the experimental data. The accuracy of the proposed model is certified by means of a meticulous comparison with the results obtained by integrating the space-time equations.

Index Terms—Nonlinear optics, semiconductor optical amplifiers, wave mixing.

I. INTRODUCTION

SEMICONDUCTOR optical amplifiers (SOAs) have been in the spotlight for many years, attracting ever growing interest in multiple areas of applications. These include all-optical signal processing in fiber-optic communication networks, cost-effective local area transmission, and, more recently, integrated silicon photonics, where SOAs are the building blocks for the implementation of large-scale integrated photonic circuits. Many of these applications rely on the mixing of the wavelength components of the propagating electric field, and their theoretical study can be performed by numerically integrating the coupled nonlinear equations describing the evolution of the electric field envelope in the longitudinal direction along the SOA, and the temporal carrier dynamics [1], [2]. Obviously, this approach is not suitable for the efficient design of an SOA, owing to the intensive computational effort that it involves. The

search for computationally efficient and analytically tractable models has yield the formulation of what is sometimes referred to as a *reduced model* for the nonlinear SOA response [3], where the space-time equations reduce to a single ordinary differential equation [3], suitable for the analytic study of multi-wave mixing (see, e.g., [3]–[5]). The formulation of a reduced model hinges upon two major assumptions. The first is that the spontaneous carrier recombination rate is proportional to the carrier spatial density, and the second is that the material gain also depends linearly on the carrier density. These assumptions emanate from early studies of semiconductor lasers. Indeed, in lasers the carrier density dynamics is characterized by small deviations from a steady state value which is set by the threshold condition of gain equalling the cavity loss. The small deviations around this value are only caused by amplified spontaneous emission (ASE) and by some spatial hole burning, which is however of little significance because in most structures the intra-cavity optical intensity is only moderately inhomogeneous. Consequently, in laser structures, gain and spontaneous emission rate can be accurately described by a linearized expression around the steady state carrier density. Early studies on SOA structures also used linear expressions for gain and carrier recombination, and in this case the linearization, albeit less accurate, found its ground on its simplicity and, more importantly, on the limited gain of legacy SOAs, which implied a limited longitudinal inhomogeneity of the optical field in the optical waveguide.

Unfortunately, these assumptions do not reflect the characteristics of modern SOAs, as is clarified in what follows. Modern SOAs may have linear gain in excess to 40 dB, implying a pronounced longitudinal inhomogeneity of the field intensity and hence of gain saturation. This may cause, in some cases, that the gain is only slightly saturated at the waveguide input, whereas it is almost zero at the waveguide output, where saturation is so high that the carrier density approaches its transparency value. When this is the case, a linear expression for the gain is reasonably accurate only if the gain does not deviate significantly from the linear expansion around the transparency carrier density over a range of values. The nowadays widely accepted forms for the dependence of the material gain on carrier density do not meet this requirement, because over such wide range of carrier density values the nonlinearity cannot be neglected, especially in quantum-well (QW) SOAs devices [6]. This makes the use of linear forms for the gain not an option for an accurate and quantitative description of the SOA dynamics. In addition, advances in material fabrication have made in modern devices the

Manuscript received October 12, 2015; revised January 15, 2016; accepted January 15, 2016. Date of publication January 17, 2016; date of current version March 18, 2016. This work was supported by DARPA under Project W911NF-14-1-0249. The work of C. Antonelli and A. Mecozzi was supported by the Italian Ministry of University and Research under ROAD-NGN Project (PRIN 2010–2011), and under Cipe resolution 135 (Dec. 21, 2012), project INnovating City Planning through Information and Communication Technologies.

C. Antonelli and A. Mecozzi are with the Department of Physical and Chemical Sciences, University of L'Aquila, L'Aquila 67100, Italy (e-mail: cristian.antonelli@univaq.it; antonio.mecozzi@univaq.it).

W. Li and L. Coldren are with the Departments of Electrical and Computer Engineering and Materials, University of California, Santa Barbara, CA 93106 USA (e-mail: teralee008@gmail.com; coldren@ece.ucsb.edu).

Color versions of one or more of the figures in this paper are available online at <http://ieeexplore.ieee.org>.

Digital Object Identifier 10.1109/JLT.2016.2519240

contribution of defect-induced carrier recombination, which is proportional to the carrier density N , negligible, with the consequence that spontaneous carrier recombination is dominated primarily by radiative recombination, whose rate is proportional to N^2 , and secondarily by Auger recombination, whose rate is proportional to N^3 [6]. This reality makes the linearization of the spontaneous recombination rate also a questionable approximation. All these arguments together suggest that the accuracy of models of the nonlinear SOA response based on linearization of the carrier recombination rate and gain may be, in state-of-the-art devices, highly inaccurate.

A natural approach to the study of wave mixing in SOAs, which closely reminds coupled-mode theories, is the one based on the derivation of evolution equations for the complex amplitudes of the field frequency components. Somewhat surprisingly, studies of wave mixing in modern SOAs (that is, SOAs characterized by a nonlinear dependence of the recombination rate and material gain on carrier density) based on this approach seem to be absent in the literature. In a couple of recent papers [7], [8], the authors assume a linear gain and a polynomial recombination rate, as it would be appropriate for bulk SOAs. However, they express the recombination rate as $R(N) = N/\tau_c(N)$, where $\tau_c(N) = N/R(N)$ has the meaning of an equivalent spontaneous carrier lifetime and, in the derivation of the coupled-mode equations, they replace $\tau_c(N)$ with some time- and space-independent value. This makes, again, the assumed carrier recombination rate linear.

Another distinctive assumption of all existing coupled-mode approaches to multi-wave mixing in SOAs is that the carrier density modulation induced by the mixing is characterized by a single harmonic component [8]. This is a reasonable assumption when a single frequency component is dominant over the others, like for instance, in four-wave mixing (FWM) experiments where a single pump and a frequency-detuned weak signal are injected into the SOA. On the contrary, this assumption is not satisfied when multiple frequency components, detuned by a few gigahertz, have comparable intensities. This configuration characterizes for instance experiments where two strong pumps are injected at frequencies $-\Omega + \omega_0$ and $\Omega + \omega_0$, and one is interested in the amplification of a weak signal injected at the central frequency ω_0 . In this case, the strongest carrier modulation occurs at the beat frequency 2Ω between the two strong pumps, but the signal amplification is mainly affected by the, possibly weaker, carrier modulation at frequency Ω . This configuration recently became of great interest because it describes the operation of a relevant class of SOA-based phase sensitive amplifiers (PSAs) [9]–[13].

In this paper, we derive coupled-mode equations describing multi-wavelength mixing in SOAs characterized by arbitrary functional dependencies of the recombination rate and material gain on carrier density. These include both QW and bulk SOAs. The proposed model, which in what follows we refer to as the *couple-mode model*, takes into account the frequency dependence of the material gain, as well as all orders of the waveguide dispersion, and accommodates input optical waveforms consisting of arbitrary combinations of multiple frequency

components.¹ The implementation of the model is illustrated in detail in the case of a QW SOA characterized by a logarithmic dependence of the optical gain on the carrier density N , and by a cubic-polynomial carrier recombination rate $R(N)$. The accuracy of the coupled-mode model is successfully tested (unlike in previous related studies) by means of a meticulous comparison with the results obtained by integrating the space-time equations of the SOA full model. Remarkably, owing to their inherent simplicity, the coupled-mode equations imply computational costs by orders of magnitude smaller than those required by the space-time equations, thus enabling the efficient characterization of multi-wave mixing in SOA structures, which would be otherwise highly impractical. We then apply the derived coupled-mode equations to studying the operation of a recently demonstrated dual-pumped PSA based on an integrated QW SOA [11]. We prove the results to be consistent with the experimental data, and confirm the excellent agreement with the results obtained by using the full SOA model.

II. COUPLED-MODE EQUATIONS FOR MULTI-WAVELENGTH PROPAGATION IN SOAs

We denote by $E(z, t)$ the slowly-varying complex envelope of the electric field propagating in the SOA in the temporal reference frame that accommodates the field group velocity v_g , corresponding to the real field

$$\mathcal{E}(z, t) = \text{Re} \left[E \left(z, t - \frac{z}{v_g} \right) e^{-i[\omega_0 t - \beta(\omega_0)z]} \right], \quad (1)$$

with ω_0 being the optical frequency. The field envelope E is normalized so that that $|E|^2$ is the optical power flowing through the transverse waveguide section. It is related to the photon flux P in photons per unit time and area through the relation

$$|E|^2 = \hbar\omega_0 S_{\text{mod}} P, \quad (2)$$

where $S_{\text{mod}} = S/\Gamma$ is the modal area of the waveguide, with S denoting the effective SOA area and Γ the optical confinement factor. The evolution of $E(z, t)$ along the SOA is governed by the familiar equation

$$\frac{\partial E}{\partial z} = \frac{1}{2} [(1 - i\alpha)\Gamma\hat{g} - \alpha_{\text{int}}] E + i\hat{\beta}E + r_{\text{sp}}, \quad (3)$$

¹We consider here only the nonlinearity that comes from carrier modulation, neglecting ultrafast nonlinearity arising from carrier heating, two photon absorption and spectral hole burning. This choice has been motivated to keep the analysis simple, and also because we are interested to cases where nonlinearity is large enough to be used in all-optical processing applications or to be an issue in applications where linearity is sought for. In these cases, the frequency detuning does not exceed a few tens of gigahertz, and in this detuning range the nonlinear modulation is mostly caused by carriers. The inclusion of ultrafast processes, however, does not pose any conceptual difficulties, and can be done along the lines of ref. [14] assuming that the gain depends on quantities other than carrier density, like, e.g., the carrier temperature for carrier heating, or the energy-resolved population of carriers for spectral hole burning, and assuming a linear decay process of these quantities towards their steady state values. The effect of carrier capture and escape processes in QW structures can be similarly taken into account by considering two distinct carrier densities, one for the confinement region and one for the QW. Also these processes, however, become of relevance for a pump-probe frequency detuning of the order of 100 GHz [15], much higher than the range of values considered here.

where α is the Henry factor, α_{int} is the SOA internal loss coefficient, and r_{sp} is the spontaneous emission noise term. By \hat{g} and $\hat{\beta}$ we denote the material gain operator and the wavenumber operator. The operator formalism allows us to conveniently accommodate the frequency dependence of the gain as well as the waveguide dispersion to any order. Within this formalism the two operators can be expressed as

$$\hat{g} = \sum_{m=0}^{\infty} \frac{1}{m!} \frac{\partial^m g(N, \omega_0)}{\partial \omega_0^m} \left(i \frac{\partial}{\partial t} \right)^m \quad (4)$$

$$\hat{\beta} = \sum_{m=2}^{\infty} \frac{1}{m!} \frac{d^m \beta(\omega_0)}{d\omega_0^m} \left(i \frac{\partial}{\partial t} \right)^m, \quad (5)$$

where $g(N, \omega)$ is the gain coefficient expressed as a function of the carrier density N and the optical frequency ω , and $\beta(\omega)$ is the frequency-dependent field propagation constant. The expressions for \hat{g} and $\hat{\beta}$ in Eqs. (4) and (5) are obtained by expanding $g(N, \omega)$ and $\beta(\omega)$ around the carrier frequency ω_0 . The fact that the sum in Eq. (5) starts from $n = 2$ is consistent with the definition of $E(z, t)$ in Eq. (1), which already accounts for the effect of $\beta(\omega_0)$ and $d\beta(\omega_0)/d\omega_0 = 1/v_g$.

The spontaneous emission noise term r_{sp} is modeled as a zero-mean, complex phase independent random process. It depends explicitly on the carrier density, besides time and space, i.e., $r_{\text{sp}} = r_{\text{sp}}(N, t; z)$. Its correlation function is [16]

$$\mathbb{E} [r_{\text{sp}}^*(N, t; z) r_{\text{sp}}(N, t'; z')] = \hbar\omega_0 R_{\text{sp}}(N, t - t') \delta(z - z'), \quad (6)$$

where by the symbol \mathbb{E} we denote ensemble averaging. Here the term $\delta(z - z')$ accounts for the fact that different longitudinal waveguide sections provide statistically independent contributions to the noise term, and [6]

$$R_{\text{sp}}(N, t' - t) = \int e^{-i(\omega - \omega_0)(t' - t)} n_{\text{sp}}(N, \omega) \Gamma g(N, \omega) \frac{d\omega}{2\pi}, \quad (7)$$

is the spontaneous emission rate into the waveguide mode and in the field propagation direction, with n_{sp} denoting the population inversion factor [6]. Spontaneous emission is a small perturbation of the propagating field, so that we may safely replace N with its temporal average, thus neglecting the effect of its small fluctuations around this value. Within this approximation the process of spontaneous emission can be modeled as a stationary process in time.

The equation for the carrier density is

$$\frac{\partial N}{\partial t} = R_J - R_{\text{rad}} - R_{\text{nr}}, \quad (8)$$

where the meaning of each of the terms at the right-hand side of the equation is discussed in what follows. The term

$$R_J = \frac{J w_a L}{V} = \frac{J}{ed}, \quad (9)$$

is the carrier injection rate into the active volume $V = SL = w_a dL$, where w_a is the active region width, L is the active region length, and d is the active region thickness. The term $R_{\text{rad}} = R_{\text{in}} + R_{\text{out}}$ is the radiative recombination rate related to

processes in which the recombination of one carrier is associated to the generation of one photon. The term R_{in} refers to processes in which emission occurs into the guided mode. By definition, this implies that $R_{\text{in}}(N)$ is related to the flux of photons flowing in the waveguide P through the balance relation

$$R_{\text{in}} S dz = S_{\text{mod}} [P(z + dz) - P(z)], \quad (10)$$

which yields

$$R_{\text{in}} = \frac{1}{\Gamma} \frac{\partial P}{\partial z}. \quad (11)$$

The processes accounted for by R_{in} includes stimulated emission and spontaneous emission within the waveguide mode (which is only a fraction of the overall spontaneous emission). The term $R_{\text{out}}(N)$ is the rate of recombinations accompanied by spontaneous emission of photons outside the waveguide mode and it can be expressed as $R_{\text{out}} = BN^2 - R_{\text{sp},\text{in}}$, where the term BN^2 is known to be an excellent approximation of the total rate of recombinations associated with spontaneous emission (inside and outside the waveguide mode) [6], and $R_{\text{sp},\text{in}}$ accounts for the rate of recombinations that produce spontaneous emission in the waveguide mode, namely it accounts for the contribution to the carrier recombination rate of the noise term r_{sp} that appears in Eq. (3). Finally, the term R_{nr} is the recombination rate of non-radiative processes, which we express as $R_{\text{nr}} = AN + CN^3$, where the linear contribution AN is mostly due to defect-induced recombination, and the cubic contribution CN^3 to Auger recombination.² By combining the various mechanisms, Eq. (8) becomes

$$\frac{\partial N}{\partial t} = -R(N) + \frac{J}{ed} + R_{\text{sp},\text{in}} - \frac{1}{\hbar\omega_0 S} \frac{\partial |E|^2}{\partial z}, \quad (12)$$

where by $R(N)$ we denote the familiar recombination rate³

$$R(N) = AN + BN^2 + CN^3. \quad (13)$$

By expanding the derivative $\partial |E|^2 / \partial z$ and using Eq. (3), Eq. (12) assumes the form

$$\frac{\partial N}{\partial t} = -R(N) + \frac{J}{ed} - \frac{1}{\hbar\omega_0 S} \text{Re} [E^* (1 - i\alpha) \Gamma \hat{g} E], \quad (14)$$

where we used the fact that $\hat{\beta}$ is a Hermitian operator, and hence it does not contribute to $\partial |E|^2 / \partial z$. The last term at the right-hand side of Eq. (14) reduces to the familiar form $\Gamma g |E|^2 / \hbar\omega_0 S$ if the gain coefficient is assumed to be frequency independent. Note that in Eq. (14), the term $R_{\text{sp},\text{in}}$ disappears because it

²We note that, while the resulting cubic polynomial expression $AN + BN^2 + CN^3$ has been shown to fit very well the experimental data in most cases [6], the one-to-one correspondence between the three terms of the polynomial and the three recombination mechanisms is not always as definite as is illustrated in the main text. For instance, in the case of non-parabolic bands (the normal case), radiative recombination is also non-parabolic and is best modeled with a bit of linear component; carrier leakage (due to finite QW barriers) has an exponential dependence and requires a polynomial fit, affecting the numerical values of A , B , and C .

³This expression of $R(N)$ is widely established and is given here for consistency with previous studies. We stress, however, that the analysis that follows does not make use of it explicitly, and rather applies to arbitrary expressions of $R(N)$.

cancels with an opposite term that—by definition—comes from $\partial|E|^2/\partial z$.

We note that Eqs. (3) and (14) can be generalized so as to include the field polarization in the analysis. While this task is rather straightforward and does not involve any conceptual challenge, we intentionally ignore polarization-related issues in order to keep the focus on the main objective of this work, which is the study of multi-wavelength propagation.

We express the multi-wavelength electric field and the carrier density as follows,

$$E(z, t) = \sum_k E_k(z) e^{-ik\Omega t}, \quad (15)$$

$$N(z, t) = N_0(z) + \sum_k \Delta N_k(z) e^{-ik\Omega t}, \quad (16)$$

where the coefficients ΔN_k must satisfy the equality $\Delta N_{-k}(z) = \Delta N_k^*(z)$ for $N(z, t)$ to be real. The term $N_0(z) + \Delta N_0(z)$ is the z -dependent time-independent value of the carrier density that characterizes the system when it achieves its stationary state, and $N_0(z)$ is defined as the solution of

$$\frac{J}{ed} = R(N_0) + \frac{\Gamma}{\hbar\omega_0 S} \sum_k g(N_0, \omega_k) |E_k|^2. \quad (17)$$

For values of the frequency spacing $\Omega/2\pi$ that exceed the SOA modulation bandwidth, the temporal fluctuations of $N(z, t)$ around its stationary value are filtered by the carrier dynamics and hence they can be treated within a perturbation approach. A consequence of this situation is that the deviation $\Delta N_0(z)$ of the stationary carrier density value from $N_0(z)$ is also a perturbation, and is small compared to $N_0(z)$. In this framework, all carrier-density dependent quantities that appear in Eqs. (3) and (14) can thus be expanded to first order with respect to $\Delta N = N - N_0$, namely

$$R(N) = R(N_0) + \frac{\Delta N}{\tau(N_0)}, \quad (18)$$

$$g(N, \omega) = g(N_0, \omega) + g_N(N_0, \omega) \Delta N, \quad (19)$$

where by the subscript N we denote differentiation with respect to N . The quantity

$$\tau(N_0) = R_N(N_0)^{-1} = \left[\frac{dR(N)}{dN} \Big|_{N=N_0} \right]^{-1}, \quad (20)$$

is the spontaneous carrier lifetime, and

$$g_N(N_0, \omega) = \frac{\partial g(N, \omega)}{\partial N} \Big|_{N=N_0}, \quad (21)$$

is the differential gain. We stress that *these are z -dependent quantities*, owing to the fact that $N_0 = N_0(z)$, and hence their values evolve along the SOA. We also notice that the effective carrier lifetime governing the dynamics of carrier modulation around the steady state value is the *differential* carrier lifetime $\tau(N_0)$ given in Eq. (20) and also introduced in [17], and not the *total* carrier lifetime $\tau_c(N_0) = N_0/R(N_0)$ used in Refs. [7]

and [8]. The difference between these two quantities is approximately a factor of 2 when the radiative bimolecular recombination BN^2 is the dominant contribution to $R(N)$, or 3 when the Auger recombination CN^3 is dominant. By inserting Eqs. (18) and (19) into Eq. (3) and Eq. (14) we obtain

$$\frac{\partial E}{\partial z} = \frac{1}{2} [(1 - i\alpha)\Gamma(\hat{g}_0 + \Delta N \hat{g}_N) - \alpha_{\text{int}}] E + i\hat{\beta} E + r, \quad (22)$$

and

$$\begin{aligned} \frac{\partial \Delta N}{\partial t} = & -\frac{\Delta N}{\tau(N_0)} - \left[R(N_0) - \frac{J}{ed} \right] \\ & - \frac{\text{Re} [E^* (1 - i\alpha)\Gamma \hat{g}_0 E]}{\hbar\omega_0 S} \\ & - \Delta N \frac{\text{Re} [E^* (1 - i\alpha)\Gamma \hat{g}_N E]}{\hbar\omega_0 S}, \end{aligned} \quad (23)$$

where the operators \hat{g}_0 and \hat{g}_N are defined as in Eq. (4), provided that $g(N, \omega)$ is replaced with $g(N_0, \omega)$ and $g_N(N_0, \omega)$, respectively.

The evolution equation for the electric field coefficient E_k is obtained by inserting the expression of the field (15) in Eq. (22) and by equating the coefficient of the term $\exp(-ik\Omega t)$ at the two sides of the resulting equation. As a result, one finds

$$\begin{aligned} \frac{dE_k}{dz} = & \left[\frac{1}{2}(1 - i\alpha)\Gamma g(N_0, \omega_k) - \alpha_{\text{int}} + i\beta(\omega_k) \right] E_k \\ & + \frac{1}{2}(1 - i\alpha) \sum_n \Delta N_{k-n} \Gamma g_N(N_0, \omega_n) E_n + r_k, \end{aligned} \quad (24)$$

where we used $\hat{g}_0 E = \sum_k g(N_0, \omega_k) E_k \exp(-ik\Omega t)$ and $\hat{g}_N E = \sum_k g_N(N_0, \omega_k) E_k \exp(-ik\Omega t)$, with $\omega_k = \omega_0 + k\Omega$. The noise term r_k is defined by

$$r_k(N; z) = \int dt e^{ik\Omega t} r_{\text{sp}}(N, t; z), \quad (25)$$

has zero mean $\langle r_k(N; z) \rangle = 0$, and its variance follows from

$$\begin{aligned} \langle r_k^*(N; z) r_h(N; z') \rangle = & \delta(z - z') \hbar\omega_0 \\ & \times \int dt \int dt' \exp[i\Omega(kt' - ht)] R_{\text{sp}}(N, t' - t). \end{aligned} \quad (26)$$

Using the stationarity of R_{sp} , we may express the above as

$$\begin{aligned} \langle r_k^*(N; z) r_h(N; z') \rangle = & \delta_{k,h} \delta(z - z') \hbar\omega_0 \\ & \times n_{\text{sp}}(N, \omega_0 + k\Omega) \Gamma g(N, \omega_0 + k\Omega). \end{aligned} \quad (27)$$

The terms $r_k(N; z')$, $k = 0, \pm 1, \pm 2, \dots$ are therefore a set of phase-independent, spatially-uncorrelated noise terms, which can be modeled as differentials of independent Wiener processes. At this point we can recast Eq. (24) in the following compact form

$$\frac{d\vec{E}}{dz} = \left[\frac{1}{2}(1 - i\alpha)\Gamma(\mathbf{G} + \mathbf{H}) - \alpha_{\text{int}}\mathbf{I} + i\mathbf{b} \right] \vec{E} + \vec{r}, \quad (28)$$

where \vec{E} and \vec{r} are column vectors constructed by stacking the electric field coefficients E_k and the noise projections r_k one on

top of another, respectively, with E_0 and r_0 occupying the central position, namely $\vec{E} = [\dots, E_2, E_1, E_0, E_{-1}, E_{-2}, \dots]^t$, and the same for \vec{r} (the superscript t stands for “transposed”). The vector \vec{E} and \vec{r} are of course infinite-dimensional, and so are the square matrices \mathbf{G} , \mathbf{H} and \mathbf{b} . Consistently with the definition of \vec{E} , we use positive and negative indices to identify the elements of these matrices, with the $(0, 0)$ element occupying the central position. In particular, \mathbf{G} and \mathbf{b} are diagonal matrices whose (k, k) elements are equal to $G_{k,k} = g(N_0, \omega_k)$ and $b_{k,k} = \beta(\omega_k) - \beta(\omega_0) - k\Omega d\beta(\omega_0)/d\omega_0$, respectively, whereas the (k, n) element of \mathbf{H} is $H_{k,n} = \Delta N_{k-n} g_N(N_0, \omega_n)$. By \mathbf{I} we denote the identity matrix (regardless of its dimensions).

We now proceed to the extraction of the carrier density coefficients ΔN_k by equating the terms proportional to $\exp(-ik\Omega t)$ at the two sides of Eq. (23), when the expression of ΔN in Eq. (16) is inserted in it. After some straightforward algebra, involving the use of Eq. (17), one obtains

$$(1 - ik\tau\Omega) \Delta N_k = - \sum_h \Delta N_h p_{k,h} + \mathcal{N}_k, \quad (29)$$

where

$$\begin{aligned} \mathcal{N}_k &= -\tau(N_0)R(N_0)(1 - \delta_{k,0}) \\ &\times \sum_n \left[\frac{(1 - i\alpha)E_{n+k}E_n^*}{P_{\text{stim}}(N_0, \omega_{n+k})} + \frac{(1 + i\alpha)E_{n+k}E_n^*}{P_{\text{stim}}(N_0, \omega_n)} \right], \quad (30) \\ p_{k,h} &= \sum_n \left[\frac{(1 - i\alpha)E_{n+k-h}E_n^*}{P_{\text{sat}}(N_0, \omega_{n+k-h})} + \frac{(1 + i\alpha)E_{n+k-h}E_n^*}{P_{\text{sat}}(N_0, \omega_n)} \right]. \quad (31) \end{aligned}$$

The quantity

$$P_{\text{sat}}(N_0, \omega) = \frac{\hbar\omega_0 S}{\tau(N_0)\Gamma g_N(N_0, \omega)} \quad (32)$$

is the familiar saturation power, although its definition accounts for the frequency dependence of the gain coefficient explicitly, and

$$P_{\text{stim}}(N_0, \omega) = R(N_0) \frac{\hbar\omega_0 S}{\Gamma g(N_0, \omega)} \quad (33)$$

is the power value above which carrier depletion is dominated by stimulated emission. We hence refer to P_{stim} as to *stimulated* power. Equation (29) can be conveniently recast in the following compact form

$$(\mathbf{I} - i\tau\Omega\mathbf{k} + \mathbf{p})\Delta\vec{N} = \vec{\mathcal{N}}, \quad (34)$$

where the (k, h) element of the matrix \mathbf{p} is equal to $p_{k,h}$, and \mathbf{k} is a diagonal matrix with diagonal elements $\kappa_{k,k} = k$. The column vectors $\Delta\vec{N}$ and $\vec{\mathcal{N}}$ are constructed (like the field vector \vec{E}) by stacking the coefficients ΔN_k and \mathcal{N}_k one on top of another, respectively, namely, $\Delta\vec{N} = [\dots, \Delta N_1, \Delta N_0, \Delta N_{-1}, \dots]^t$ and $\vec{\mathcal{N}} = [\dots, \mathcal{N}_1, 0, \mathcal{N}_{-1}, \dots]^t$. The coefficients N_0 and ΔN_k are hence obtained for a given electric field state by solving Eqs. (17) and (34). These are the most general coupled-mode equations accounting for any functional dependence of the recombination

rate and material optical gain on carrier density, as well as for the frequency dependence of the gain and waveguide dispersion.

III. IMPLEMENTATION OF THE COUPLED-MODE EQUATION MODEL IN REALISTIC SOA STRUCTURES

As is customarily done in most studies of practical relevance, where the waveguide dispersion and the frequency dependence of the gain coefficient have been shown to play a minor role, in this section we neglect chromatic dispersion, as well as higher-order dispersion, and assume frequency-independent gain. With this simplification the matrices \mathbf{G} , \mathbf{H} , and \mathbf{p} become frequency-independent and assume a very convenient form, as is shown in what follows. We also neglect the presence of spontaneous emission noise terms, whose implications on the SOA performance, chiefly on the SOA noise figure, will be the subject of future work.

The multi-wavelength propagation model introduced in the previous section involves an infinite number of coefficients E_k and ΔN_k , a situation that is obviously incompatible with its implementation in any numerical platform. However, as will be shown in the next section, high-order coefficients (namely E_k and ΔN_k coefficients with large values of $|k|$) provide a negligible contribution to the solution of Eqs. (17), (28), and (34), and hence they can be omitted by truncating the vectors \vec{E} and $\Delta\vec{N}$. The truncation of \vec{E} and $\Delta\vec{N}$ requires of course that all matrices involved in Eqs. (28) and (34) be also truncated accordingly. In what follows we provide explicit expressions for those matrices and discuss the procedure that allows the efficient computation of \vec{E} and $\Delta\vec{N}$.

The truncation procedure of the infinite set of equations (28) can be performed in a number of ways. One possible approach is assuming that $E_k(z) = 0$ for $|k| > M$. Here M is an integer number that can be determined self consistently by checking that the integration of the equations for $M \rightarrow M + 1$ yields indistinguishable results. This assumption implies $\Delta N_k(z) = 0$ for $|k| > 2M$, owing to the absence of beat terms at frequency offsets larger than $2M\Omega$. A simpler yet equally accurate approach is to assume that the carrier density coefficients $\Delta N_k(z)$ are also zero at frequency offsets greater than $M\Omega$. Here we adopt the latter approach, within which Eqs. (15) and (16) specialize to

$$E(z, t) = \sum_{k=-M}^M E_k(z) e^{-ik\Omega t}, \quad (35)$$

$$N(z, t) = N_0(z) + \sum_{k=-M}^M \Delta N_k(z) e^{-ik\Omega t}. \quad (36)$$

Accordingly, the field vector \vec{E} and carrier density modulation vector $\Delta\vec{N}$, consist of $(2M + 1)$ components. Matrices \mathbf{G} and \mathbf{H} in Eq. (28) become $(2M + 1) \times (2M + 1)$ matrices. In particular, owing to the assumption of frequency-flat gain, one can readily verify the equalities $\mathbf{G} = g(N_0)\mathbf{I}$, and $\mathbf{H} = g_N(N_0)\mathbf{T}(\Delta\vec{N})$, where by $\mathbf{T}_{2M+1}(\Delta N_k)$ we denote a Hermitian-symmetric Toeplitz matrix [18]. Below we give the expression of $\mathbf{T}_{2M+1}(\Delta N_k)$ in the case $M = 2$ for illustration

purposes,

$$\mathbf{T}_5(\Delta N_k) = \begin{bmatrix} \Delta N_0 & \Delta N_1 & \Delta N_2 & 0 & 0 \\ \Delta N_1^* & \Delta N_0 & \Delta N_1 & \Delta N_2 & 0 \\ \Delta N_2^* & \Delta N_1^* & \Delta N_0 & \Delta N_1 & \Delta N_2 \\ 0 & \Delta N_2^* & \Delta N_1^* & \Delta N_0 & \Delta N_1 \\ 0 & 0 & \Delta N_2^* & \Delta N_1^* & \Delta N_0 \end{bmatrix}. \quad (37)$$

The neglect of the waveguide dispersion yields $\mathbf{b} = 0$, and hence Eq. (28) simplifies to

$$\frac{d\vec{E}}{dz} = \left[\frac{(1 - i\alpha)g(N_0) - \alpha_{\text{int}}}{2} \mathbf{I} + \mathbf{T}_{2M+1}(\Delta N_k) \right] \vec{E}, \quad (38)$$

where N_0 is the solution of

$$\frac{J}{ed} = R(N_0) \left[1 + \frac{|\vec{E}|^2}{\tau P_{\text{stim}}(N_0)} \right], \quad (39)$$

with

$$P_{\text{stim}}(N_0) = R(N_0) \frac{\hbar\omega_0 S}{\Gamma g(N_0)}. \quad (40)$$

The expression for the carrier density modulation vector $\Delta\vec{N}$ simplifies to

$$\Delta\vec{N} = -\frac{\tau R(N_0)}{P_{\text{stim}}(N_0)} \left[\mathbf{I} - \tau\Omega\mathbf{k} + \frac{\mathbf{T}_{2M+1}(C_k)}{P_{\text{sat}}(N_0)} \right]^{-1} \vec{C}, \quad (41)$$

where

$$P_{\text{sat}}(N_0) = \frac{\hbar\omega_0 S}{\tau(N_0)\Gamma g_N(N_0)}, \quad (42)$$

and where C_k is the discrete autocorrelation function of \vec{E} , namely

$$C_k = \sum_{n=-M}^M E_{n+k} E_n^*, \quad (43)$$

in which we assume $E_n = 0$ for $|n| > M$. The expression of \vec{C} in the case $M = 2$ is

$$\vec{C} = [C_2, C_1, C_0, C_1^*, C_2^*]^t, \quad (44)$$

and that of $\mathbf{T}_5(C_k)$ is

$$\mathbf{T}_5(C_k) = \begin{bmatrix} C_0 & C_1 & C_2 & C_3 & C_4 \\ C_1^* & C_0 & C_1 & C_2 & C_3 \\ C_2^* & C_1^* & C_0 & C_1 & C_2 \\ C_3^* & C_2^* & C_1^* & C_0 & C_1 \\ C_4^* & C_3^* & C_2^* & C_1^* & C_0 \end{bmatrix}, \quad (45)$$

where we used $C_{-k} = C_k^*$, as can be readily verified by inspecting Eq. (43).

The numerical integration of the coupled-equations involves a three-step procedure for the transition from z to $z + \Delta z$, given the field vector $\vec{E}(z)$. These are:

- 1) Find the value of $N_0(z)$ by solving Eq. (39);
- 2) Extract the carrier density vector $\Delta\vec{N}(z)$ as in Eq. (41);

TABLE I
SOA PARAMETERS

Description	Value	Units
Linear recombination coefficient A	10^6	s^{-1}
Bimolecular recombination coefficient B	0.3×10^{-10}	cm^3/s
Auger coefficient C	3.3×10^{-29}	cm^6/s
Optical confinement factor Γ	9.7%	
Linewidth enhancement factor α	5	
Optical wavelength λ_0	1561	nm
Group velocity v_g	8.33×10^9	cm/s
Active region width w_a	2×10^{-4}	cm
Active region thickness d	65×10^{-7}	cm
Active region length L	0.1	cm
Gain coefficient g_0	1800	cm^{-1}
Transparency carrier density N_{tr}	2×10^{18}	cm^{-3}
SOA internal loss α_{int}	5	cm^{-1}
Injection current density J	3.4×10^3	A/cm ²
Frequency spacing $\Omega/2\pi$	8.6	GHz

- 3) Evaluate the field vector $\vec{E}(z + \Delta z)$ by solving Eq. (38) from z to $z + \Delta z$ while using the values of N_0 and ΔN_k obtained in steps 1 and 2, according to

$$\vec{E}(z + \Delta z) = \exp \left\{ \frac{(1 - i\alpha)g[N_0(z)] - \alpha_{\text{int}}}{2} \Delta z \right\} \exp \{ \mathbf{T}_{2M+1}[\Delta N_k(z)] \Delta z \} \vec{E}(z). \quad (46)$$

A. Model Validation

In this section we test the accuracy of the proposed multi-wavelength propagation model against the results obtained by integrating the full model' space-time equations (3) and (14). To this end we consider a QW SOA, characterized by the following logarithmic functional dependence of the gain coefficient on carrier density [6]

$$g(N) = g_0 \log \left(\frac{N}{N_{\text{tr}}} \right), \quad (47)$$

where g_0 is a gain parameter and N_{tr} is the carrier density required for transparency.⁴ The expansion of the gain function is in this case $g(N) \simeq g(N_0) + g_N(N_0)\Delta N$, with

$$g(N_0) = g_0 \log \left(\frac{N_0}{N_{\text{tr}}} \right), \quad g_N(N_0) = \frac{g_0}{N_0}. \quad (48)$$

The physical and operational parameters of the SOA are listed in Table I (we note that the SOA is operated with the injection current density $J = 8.5J_{\text{tr}}$, where $J_{\text{tr}} = ed(AN_{\text{tr}} + BN_{\text{tr}}^2 + CN_{\text{tr}}^3)$ is the injection current density required for transparency). The SOA is injected with a three-wavelength optical signal characterized by the complex envelope

$$E_{\text{in}}(t) = \sqrt{W_1} e^{-i\Omega t} + \sqrt{W_0} + \sqrt{W_{-1}} e^{i\Omega t} \quad (49)$$

with $W_1 = W_{-1} = -2$ dBm, and $W_0 = -7$ dBm. For this set of parameters we solved the coupled-mode equations (38), (40), and (41) with the input field vector $\vec{E}_{\text{in}} = [\dots, 0, \sqrt{W_1}, \sqrt{W_0}]$,

⁴Of course, the use of different functional forms of $g(N)$, for instance the more accurate three parameter expression $g(N) = g_0 \ln[(N + N_s)/(N_{\text{tr}} + N_s)]$ also reported in [6], is fully equivalent in terms of model complexity.

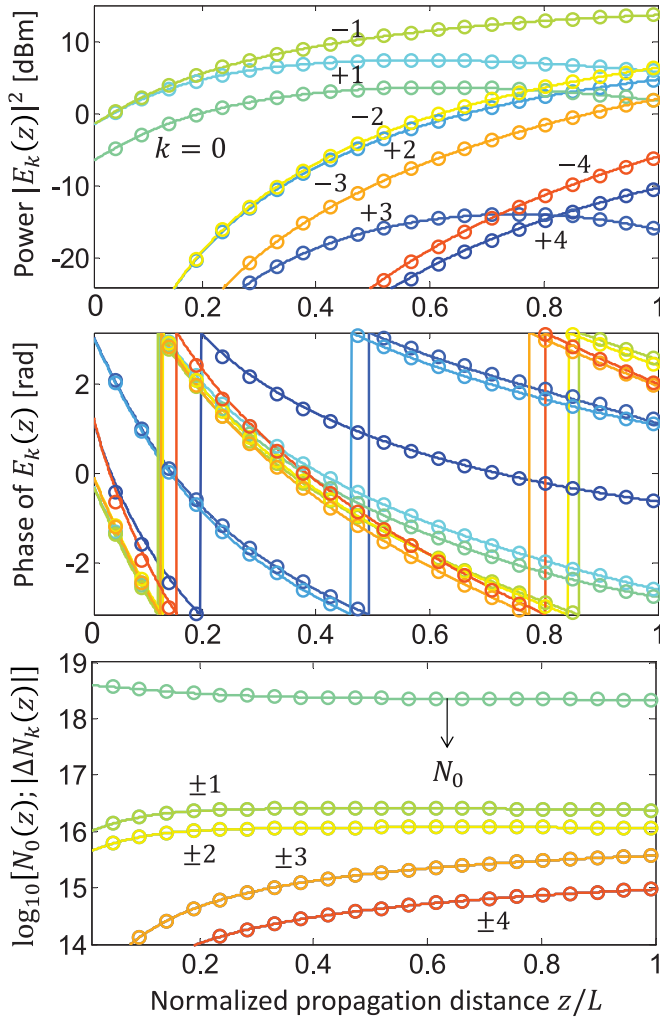


Fig. 1. Intensity (top panel) and phase (bottom panel) of the field components E_k versus normalized propagation distance z/L for the displayed values of k and for the SOA parameters' values in Table I. Solid curves refer to the coupled-mode model, while circles were obtained by solving the space-time equations of the full model.

$\sqrt{W_{-1}}, 0, \dots]^t$. We used $M = 6$ and checked that larger values of M yield indistinguishable results. We then integrated the full model's equations (3) and (14) with the procedure described in [19], and extracted the coefficients $E_k(z)$ from the numerical solution $E_{\text{num}}(z, t)$ according to

$$E_k(z) \leftrightarrow \frac{\Omega}{2\pi} \int_{t_0}^{2\pi/\Omega} E_{\text{num}}(z, t) e^{ik\Omega t} dt, \quad (50)$$

where by t_0 we denote any time at which the system achieved its stationary state. The results are shown in Fig. 1. In the top panel we plot by solid curves the intensities of the coefficients $E_k(z)$ versus the normalized propagation distance z/L for values of k ranging between $k = -4$ and $k = 4$. By circles we plot the results obtained with the full model. The excellent accuracy of the coupled-mode model is self-evident. Interestingly, the figure shows that the coupled-mode model is accurate in describing the formation of FWM components that eventually (at the SOA output) exceed some of the input components. The center panel of the same figure shows the corresponding phases

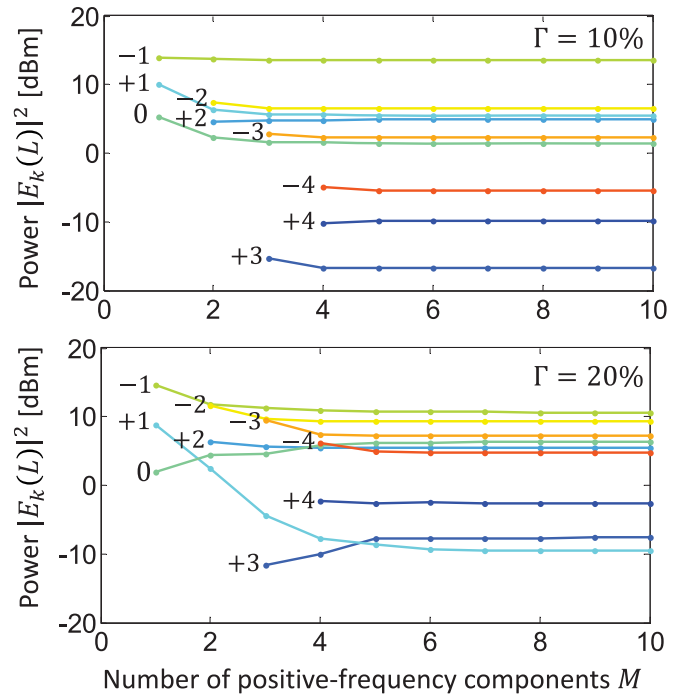


Fig. 2. Intensities of field components E_k at the SOA output $|E_k(L)|^2$, as obtained by using the coupled-mode model, for increasing values of M . Each curve corresponds to a specific value of k and hence it originates at $|k| = M$. The top panel refers to the set of parameters listed in Table I and used in Fig. 1, whereas in the bottom panel the optical confinement factor was increased from 10% to 20%.

of the field coefficients E_k (more precisely the solid curves are the plot of $\text{Phase}[E_k(z)] + k\Omega z/v_g$, where the second term accounts for the fact that the coefficients $E_k(z)$ characterize the field envelope in the time reference delayed by z/v_g). The lower panel provides a direct validation of the condition $|\Delta N_k| \ll N_0$, which was assumed in the perturbation analysis. The top circles show the time-averaged carrier density (in a logarithmic scale) extracted from the full model results. Although this quantity is described in the coupled-mode model by $N_0 + \Delta N_0$, we compare it with N_0 , which is shown as a solid curve. The excellent agreement between the two plotted quantities is a proof of the condition $\Delta N_0 \ll N_0$. Lower curves and markers are plots of $|\Delta N_k|$ for values of $|k|$ ranging between 1 and 4 (we recall that $|\Delta N_k| = |\Delta N_{-k}|$). The plot shows that the absolute value of the coefficients ΔN_k is more than two orders of magnitude smaller than N_0 , thus confirming the condition $|\Delta N_k| \ll N_0$, also for $|k| > 0$. Moreover, the excellent agreement between the full model and the coupled-mode model validates the perturbation approach for arbitrary magnitude of the perturbations.

We stress that the coupled-mode model offers considerably greater computational efficiency, as compared to the full time domain model. In the specific example of Fig. 1, the integration time of the coupled-mode equations was more than two orders of magnitude smaller than the integration time required by the space-time equations, using in both cases in-house developed MATLAB routines run on the same workstation.

In Fig. 2 we illustrate the dependence of the coupled-mode model's results on the number of field coefficients that are

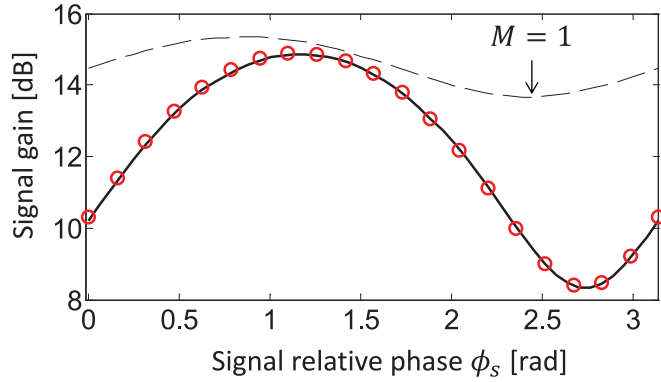


Fig. 3. Dual-pumped SOA-based PSA's gain versus the relative phase of the input signal ϕ_s introduced in Eq. (55). The SOA parameters used in the numerical computation are those given in Table I, the input pump powers were set to $W_{P_1} = W_{P_2} = -2$ dBm, and the input signal power to $W_s = -22$ dBm. The solid curve refers to the coupled-mode model with $M = 4$ (larger values of M yield indistinguishable results), while the circles were obtained by integrating the space-time equations of the full model. The dashed curve shows the results obtained with the coupled-mode model by propagating only the pump and signal components, namely by setting $M = 1$.

considered. In the top panel we plot the output intensities $|E_k(L)|^2$ evaluated by solving the coupled-mode equations for increasing values of M , with each curve corresponding to a different value of k . Since the accounting for the frequency component E_k dictates that $M \geq |k|$, the curve referring to E_k originates at $M = |k|$. The plot shows that in the numerical example considered here the results of the coupled-mode equations for the component E_k become accurate (that is, the corresponding curve in the figure becomes flat) for M exceeding $|k|$ by a one or two units. However, it should be pointed out that the convergence to the correct result is affected by the specific SOA parameters' value and may be slower. This is shown in the lower panel of the Fig. 2, where the same curves plotted in the top panel are re-calculated by increasing the SOA optical confinement factor from 10% to 20% and by leaving the other SOA parameters unchanged. In this example, it can be seen that using $M < 6$ may yield an error in the calculation of $|E_1(L)|^2$ up to a factor of 100.

The SOA length assumed in this section for the validation of the coupled-mode model is intermediate between the typical length of “ultra-short” SOAs ($L < 0.5$ mm) and that of “ultra-long” SOAs ($L > 1$ mm). We note that while the accuracy of the coupled-mode model is not affected in the case of shorter SOAs, the model may require some improvement in the case of ultra-long SOAs, where one needs to take into account the spatial dependence of the injection current, as well as its dependence on the local carrier density [20].

IV. APPLICATION OF THE MODEL: DUAL-PUMPED SOA-BASED PSA

In this section we apply the coupled-mode model to the study of the dual-pumped SOA-based PSA presented in [11]–[13]. The goal of this exercise is two-folded. On the one hand we aim to show that the phase-sensitive gain value obtained with the coupled-mode model assuming realistic SOA parameters is

consistent with the experimentally obtained value. On the other hand, we show explicitly that by restricting the coupled-mode model to the pump and signal components only, as is sometimes done [21], yields significantly incorrect results when a realistic dependence of the amplifier gain on carrier density is used.

The waveform at the input of a PSA of the kind considered here can be expressed as

$$E_{\text{in}}(t) = e^{i\phi_1} \sqrt{W_1} e^{-i\Omega t} + e^{i\phi_0} \sqrt{W_0} + e^{i\phi_{-1}} \sqrt{W_{-1}} e^{i\Omega t}, \quad (51)$$

where by W_1 and W_{-1} we denote the optical powers of the two pumps and by ϕ_1 and ϕ_{-1} their absolute phases. The field component at the central frequency represents the input signal component. By removing in all components the immaterial average phase of the two pumps

$$\phi_c = (\phi_1 + \phi_{-1})/2, \quad (52)$$

and denoting by

$$\phi_s = \phi_0 - \phi_c \quad (53)$$

the input signal phase relative to ϕ_c , the input field envelope can be expressed as

$$E_{\text{in}}(t) = e^{i\phi_p} \sqrt{W_1} e^{-i\Omega t} + e^{i\phi_s} \sqrt{W_0} + e^{-i\phi_p} \sqrt{W_{-1}} e^{i\Omega t}, \quad (54)$$

where $\phi_p = (\phi_1 - \phi_{-1})/2$. We further note that the effect of ϕ_p is limited to introducing an immaterial time shift $t_p = \phi_p/\Omega$, and hence it can be safely set to $\phi_p = 0$. We therefore solve the space-time equations using the following input waveform,

$$E_{\text{in}}(t) = \sqrt{W_{P_1}} e^{-i\Omega t} + e^{i\phi_s} \sqrt{W_s} + \sqrt{W_{P_2}} e^{i\Omega t}, \quad (55)$$

and the coupled-mode equations with the input field vector

$$\vec{E}_{\text{in}} = [\dots, 0, \sqrt{W_{P_1}}, e^{i\phi_s} \sqrt{W_s}, \sqrt{W_{P_2}}, 0, \dots]^t. \quad (56)$$

The key quantity that characterizes the performance of the PSA under scrutiny is the dependence of the signal gain on the phase ϕ_s . In Fig. 3 we plot the gain $G_s(\phi_s) = |E_s(L)|^2/W_s$ (in decibels) as a function of ϕ_s , where in the case of the full model the term $E_s(L)$ is extracted from the numerical solution $E_{\text{num}}(L, t)$ according to Eq. (50) with $z = L$. The SOA parameters used in the numerical example are those given in Table I. The input pump powers were set to $W_{P_1} = W_{P_2} = -2$ dBm, and the input signal power to the much smaller value $W_s = -22$ dBm. The solid curve is obtained by integrating the coupled-mode model with $M = 4$, whereas the circles refer to the space-time model. The excellent agreement between the coupled-mode model and the space-time model, like in the previous section, is self-evident. The thin dashed curve in Fig. 3 shows the result obtained with the coupled-mode model by including only the pump and signal field components, that is by using $M = 1$. The plot shows that the neglect of high-order FWM products yields higher gain values and a lower phase dependent gain.

We now proceed to compare the results of the coupled-mode model with the experimental data reported in ref. [13], wherein all the details concerning the experiment can be found.

The comparison between the theory and the data is performed by looking at the dependence of the PSA gain on the input signal relative phase ϕ_s of the kind shown in Fig. 3. To this end, we

note that the numerical values of the SOA parameters listed in Table I are those estimated for one of the devices tested in [13], and specifically for the device with a phase dependent gain of about 6.3 dB. Some of the parameters were directly taken from the device geometry, like the active region length and width. The active region thickness was taken to be 65 nm to reflect the fact that the active region of the device consisted of 10 InP/InGaAsP QWs of 6.5 nm width each. Some of the parameters were estimated by independent analysis, like for instance the value of $\Gamma \simeq 10\%$, which was extracted from the mode profile given by a finite-difference-method-based electromagnetic solver. The value of the transparency current density used in simulations is $J_{th} = 0.43 \text{ kA/cm}^2$, versus the measured value of about 1 kA/cm^2 . This implies an injection efficiency of about 43%, which includes the loss caused by lateral current spreading in the waveguide region and the carrier trapping efficiency in the QWs. The values for the gain coefficient g_0 and for the coefficients A , B and C are those typical for the InP/InGaAsP MQW active region of the SOA used in the experiment [6], [13]. The waveguide internal loss was also set to the typical value of $\alpha_{int} = 5 \text{ cm}^{-1}$ measured in good quality devices. The linewidth enhancement factor $\alpha = 5$ is also within the typical range of values for devices of this type. With these parameters, the model predicts about 59 dB of linear gain, whereas the measured linear gain of the device under test was about 48.5 dB [13]. The 10 dB difference can, however, be safely attributed to gain compression induced by ASE—neglected in the model but significant for zero input in devices with high linear gain—and to thermal effects within the waveguide.

The comparison between the theoretical curve shown in Fig. 3 and the data requires some care. More specifically, since the way in which the experiment is performed does not allow a precise measurement of the input signal power, in this comparison we look at the output signal power (rather than at the gain). In the logarithmic scale, this simply requires adding a bias to the theoretical PSA gain. The relative signal phase ϕ_s defined in Eq. (53) is also not known directly. Indeed in the experiment, the phase of the input signal is controlled by passing the signal through a tuning region prior to the injection into the SOA. The phase change of the signal is proportional to the square root of the current I_ϕ injected in the tuning region. A calibration procedure allowed to establish, for I_ϕ between 1 and 2 mA, the relation $\phi_0 - \phi_1 = \pi\chi\sqrt{I_\phi}$ with $\chi \simeq 1 \text{ mA}^{-1/2}$. As a result, the relation between the signal relative phase ϕ_s and the measured control current I_ϕ , $\phi_s = \pi\chi\sqrt{I_\phi} + \phi_b$, obtained using the definition of ϕ_s in Eq. (53), contains the unknown bias $\phi_b = (\phi_1 - \phi_{-1})/2$, which also needs to be added to the theoretical signal phase in order to facilitate the comparison between the theory and the data.

In Fig. 4 we plot the output signal power versus the square-root injection current $\sqrt{I_\phi}$. The markers refer to the experimental results, and they were taken from [13, Fig. 26(a)]. The solid curve is obtained from the curve plotted in Fig. 3 by shifting the vertical and the horizontal axes, so as to fit the data, as discussed in the previous paragraph. The agreement between theory and experiment is self evident. We remark that such good agreement cannot be obtained by using the conventional three-wave

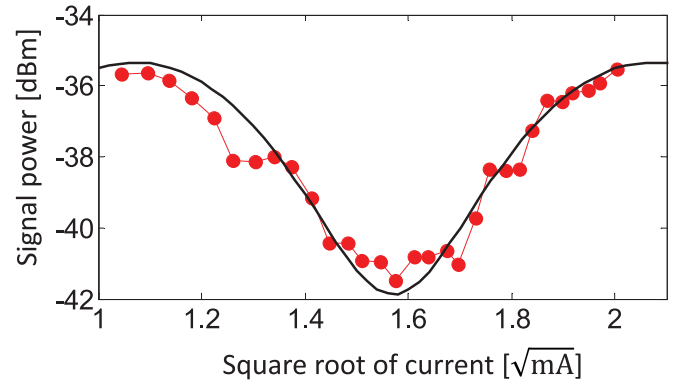


Fig. 4. Measured relationship among the signal power, the signal phase and the square root of the current applied to the phase tuner (see ref. [13]), together with the curve of Fig. 3, suitably re-centered to fit the data.

model (corresponding to the case $M = 1$ in our theory and used in ref. [21]) where the high-order harmonics generated by the nonlinear interaction between the signal and the two pump are neglected, unless unrealistic values for the device parameters are assumed.

V. CONCLUSION

To conclude, we derived a couple-mode model for multi-wave mixing in SOAs characterized by arbitrary functional dependencies of the recombination rate and material gain on carrier density. The model takes into account the frequency dependence of the material gain, as well as all orders of the waveguide dispersion, and accommodates input fields consisting of arbitrary combinations of multiple frequency components. We showed that the conventional approach assuming a limited number of generated FWM components gives inaccurate results when two waveforms of similar intensities are injected into the SOA. In this case, our model gives highly accurate results if a sufficient number of generated components are taken into account, as we showed by direct comparison with full time-domain simulations. We applied the coupled-mode model to studying the operation of a recently demonstrated dual-pumped PSA based on an integrated QW SOA [11]–[13], and showed that the outcome of the model is consistent with the experimental results.

REFERENCES

- [1] M. J. Connelly, "Wide-band steady-state numerical model and parameter extraction of a tensile-strained Bulk semiconductor optical amplifier," *IEEE J. Quantum Electron.*, vol. 43, no. 1, pp. 47–56, Jan. 2007.
- [2] A. R. Totović, J. V. Crnjanski, M. M. Krstić, and D. M. Gvozdić, "Numerical study of the small-signal modulation bandwidth of reflective and traveling-wave SOAs," *J. Lightw. Technol.*, vol. 33, no. 13, pp. 2758–2764, Jul. 1, 2015.
- [3] G. P. Agrawal, "Population pulsations and nondegenerate four-wave mixing in semiconductor lasers and amplifiers," *J. Opt. Soc. Amer. B*, vol. 5, pp. 147–159, Jan. 1988.
- [4] A. Mecozzi, "Analytical theory of four-wave mixing in semiconductor amplifiers," *Opt. Lett.*, vol. 19, pp. 892–894, Jun. 15, 1994.
- [5] A. Mecozzi and J. Mørk, "Saturation induced by picosecond pulses in semiconductor optical amplifiers," *J. Opt. Soc. Amer. B*, vol. 14, pp. 761–770, Apr. 1997.
- [6] L. A. Coldren, S. W. Corzine, and M. L. Mašanović, *Diode Lasers and Photonic Integrated Circuits* (ser. Microwave and Optical Engineering), 2nd ed. Hoboken, NJ, USA: Wiley, 2012, ch. 2, 4.

- [7] P. P. Baveja, D. N. Maywar, and G. P. Agrawal, "Interband four-wave mixing in semiconductor optical amplifiers with ASE-enhanced gain recovery," *IEEE J. Sel. Topics Quantum Electron.*, vol. 18, no. 2, pp. 899–908, Mar./Apr. 2012.
- [8] M. A. Summerfield and R. S. Tucker, "Frequency-domain model of multiwave mixing in bulk semiconductor optical amplifiers," *IEEE J. Sel. Topics Quantum Electron.*, vol. 5, no. 3, pp. 839–850, May/June 1999.
- [9] P. Frascella, S. Sygletos, F. C. Garcia Gunning, R. Weerasuriya, L. Grüner-Nielsen, R. Phelan, J. O'Gorman, and A. D. Ellis, "DPSK signal regeneration with a dual-pump nondegenerate phase-sensitive amplifier," *IEEE Photon. Technol. Lett.*, vol. 23, no. 8, pp. 516–518, Apr. 2011.
- [10] A. D. Ellis and S. Sygletos, "Phase sensitive signal processing using semiconductor optical amplifiers," presented at the Optical Fiber Communication Conf./Nat. Fiber Optic Engineers Conf., Anaheim, CA, USA, 2013, paper OW4C.1.
- [11] W. Li, M. Lu, L. Johansson, M. L. Mašanović, D. Dadic, S. Arafin, and L. Coldren, "First demonstration of an integrated photonic phase-sensitive amplifier," presented at the Conf. Lasers Electro Optics, San Jose, CA, USA, paper SW4N.5.
- [12] L. A. Coldren, W. Li, A. Mecozzi, M. Lu, S. Arafin, M. Vasilyev, D. Dadic, and L. A. Johansson, "Single-chip dual-pumped SOA-based phase-sensitive amplifier at 1550 nm," presented at the Summer Topicals Meeting Series, Jul. 13–15, 2015, pp. 88–89.
- [13] W. Li, M. Lu, A. Mecozzi, M. Vasilyev, S. Arafin, D. Dadic, L. A. Johansson, L. A. Coldren, "First monolithically integrated dual-pumped phase-sensitive amplifier chip based on a saturated semiconductor optical amplifier," *IEEE J. Quantum Electron.*, vol. 52, no. 1, pp. 1–12, Jan. 2016.
- [14] A. Mecozzi and J. Mørk, "Saturation effects in nondegenerate four-wave mixing between short optical pulses in semiconductor laser amplifiers," *IEEE J. Sel. Topics Quantum Electron.*, vol. 3, no. 5, pp. 1190–1207, Oct. 1997.
- [15] R. Paiella, G. Hunziker, and K. J. Vahala, "Quantum-well capture and inter-well transport in semiconductor active layers," *Semicond. Sci. Technol.*, vol. 14, pp. R17–R25, 1999.
- [16] C. W. Gardiner, *Handbook of Stochastic Methods* (ser. Synergetics), vol. 13, 2nd ed. Berlin, Germany: Springer-Verlag, 1985.
- [17] L. A. Coldren, S. W. Corzine, and M. L. Mašanović, *Diode Lasers and Photonic Integrated Circuits* (ser. Microwave and Optical Engineering), 2nd ed. Hoboken, NJ, USA: Wiley, 2012, ch. 5, p. 257.
- [18] A. Böttcher and S. M. Grudsky, *Toeplitz Matrices, Asymptotic Linear Algebra, and Functional Analysis*. Basel, Switzerland: Birkhäuser, 2012.
- [19] J. W. D. Chi, L. Chao, and M. K. Rao, "Time-domain large-signal investigation on nonlinear interactions between an optical pulse and semiconductor waveguides," *IEEE J. Quantum Electron.*, vol. 37, no. 10, pp. 1329–1336, Oct. 2001.
- [20] P. Morel and A. Sharaiha, "Wideband time-domain transfer matrix model equivalent circuit for short pulse propagation in semiconductor optical amplifiers," *IEEE J. Quantum Electron.*, vol. 45, no. 2, pp. 103–116, Feb. 2009.
- [21] W. Yang, T. Cao, Y. Yu, L. Shi, X. Zhang, and D. Huang, "Theoretical analysis and experimental investigation of degenerate phase sensitive amplification in a semiconductor optical amplifier," *J. Lightw. Technol.*, vol. 33, no. 19, pp. 4001–4007, Oct. 1, 2015.

Cristian Antonelli received the M.Sc. and Ph.D. degrees in electrical engineering from the University of L'Aquila, L'Aquila, Italy, in 2002 and 2006, respectively. During his graduate studies, he worked on the "Hinge Model" for the time dynamics of PMD in lightwave systems within a collaboration with AT&T Labs, Middletown, NJ, USA, where he was a Visiting Scientist in the summers of 2004 and 2005. In 2006, he spent six months with the Research Laboratory of Electronics, Massachusetts Institute of Technology, Cambridge, MA, USA, performing research on the theory of mode-locked fiber lasers. Since 2007, he has been a Senior Research Scientist first at CNISM, the Italian Interuniversity Consortium for the physics of matter, and then at the University of L'Aquila. In April 2014, he joined the Department of Physical and Chemical Sciences of the same university as an Assistant Professor. His research interests include the modeling and characterization of fiber-optic communication systems, including PMD and PDL, fundamental energy consumption limits, semiconductor optical amplifier-based devices, and linear and nonlinear propagation effects in space-division multiplexed transmission. He is currently serving as a TCP Member for OFC 2016, as well as an Associate Editor for the JLT.

Antonio Mecozzi (M'98–SM'00–F'03) is a Professor and the Director of the Department of Physical and Chemical Sciences at the University of L'Aquila, L'Aquila, Italy. Previously, he worked for 15 years in the Optical Communication Division of Fondazione Ugo Bordoni, Rome. He was a Visiting Scientist of the EECS Department and the Research Laboratory of Electronics of MIT from 1991 to 1992. His areas of research interests include studies on soliton transmission, laser mode-locking, nonlinear propagation in single and multimode fibers, modal dispersion in multimode fibers, physics and applications of semiconductor optical amplifiers, and optical amplification and noise. He holds numerous patents and more than 160 publications in refereed scientific journals. He is currently serving as an Associate Editor for *Optics Express*. He is a Fellow of the Optical Society of America.

Wangzhe Li received the Ph.D. degree from the University of Ottawa, Ottawa, ON, Canada, in 2013 working on the photonic generation of microwave and millimeter wave signals, and then joined the University of California, Santa Barbara, CA, USA, as a Postdoctoral Scholar where he has been working on integrated optical phase-sensitive amplifiers.

Larry A. Coldren (S'67–M'72–SM'77–F'82–LF'12) received the Ph.D. degree in electrical engineering from Stanford University, Stanford, CA, USA, in 1972. After 13 years in the research area with Bell Laboratories, he joined the University of California (UCSB), Santa Barbara, CA, in 1984. He is the Fred Kavli Professor of optoelectronics and sensors and holds appointments with the Departments of Materials and Electrical and Computer Engineering. From 2009 to 2011, he was the Dean of the College of Engineering. In 1990, he cofounded Optical Concepts, later acquired as Gore Photonics, to develop novel VCSEL technology, and, in 1998, he cofounded Agility Communications, later acquired by JDSU, to develop widely tunable integrated transmitters. At UCSB, he worked on multiple-section widely tunable lasers and efficient vertical-cavity surface-emitting lasers (VCSELs). More recently, his group has developed high-performance InP-based photonic integrated circuits as well as high-speed VCSELs. He has authored or coauthored more than thousand journal and conference papers. He has also coauthored eight book chapters, a widely used textbook, and has been issued 65 patents. He received the 2004 John Tyndall, 2009 Aron Kressel, 2014 David Sarnoff, and 2015 IPRM Awards, and he is a Fellow of the OSA and IEE, and a Member of the National Academy of Engineering.